Diagnostic ability of retinal nerve fiber layer maps to detect localized retinal nerve fiber layer defects

JW Shin, KB Uhm, WJ Lee and YJ Kim

Department of Ophthalmology, Hanyang University College of Medicine, Seoul, Korea

Correspondence:
KB Uhm, Department of Ophthalmology, Hanyang University College of Medicine, Haengdang 1-dong, Seongdong-gu, Seoul 133-792, Korea.
Tel.: +82 2 22908570;
Fax: +82 2 22918517.
E-mail:
kbuhm@hanyang.ac.kr

Abstract

Purpose To evaluate and compare the diagnostic ability of spectral domain optical coherence tomography (SD-OCT) for detecting localized retinal nerve fiber layer (RNFL) defects in topographic RNFL maps and circumpapillary RNFL (cpRNFL) thickness measurements.

Methods Sixty-four eyes with localized RNFL defects in red-free RNFL photographs and 72 healthy eyes were included. All participants were imaged with SD-OCT. The area and angular width of the localized RNFL defects were measured with ImageJ software on RNFL thickness map, significance map (yellow pixels, <5% level), and red-free RNFL photographs. The sensitivity, specificity, and area under the receiver operating characteristic curves (AUCs) were calculated for cpRNFL thickness, macular inner retina thickness, and RNFL maps (thickness, significance) according to the quantitative measurements and a <5% level of classification to distinguish eyes with localized RNFL defects from healthy eyes.

Results RNFL thickness map (sensitivity 96.9–98.4%, specificity 86.1–98.6%, and AUCs 0.915–0.992) and significance map (sensitivity 96.9–98.4%, specificity 88.9–95.8%, and AUCs 0.937–0.983) showed superior performance in detecting localized RNFL defects compared with other parameters (*P*-value 0.001–0.024) except for 36 sector cpRNFL thickness (sensitivity 92.2%, specificity 87.5%, and AUCs 0.898; *P*-value 0.080–0.545). The sensitivity for detecting RNFL defects was related to the angular width, area, and depth of the RNFL defects in the cpRNFL (4 sector, 12 sector) and macular inner retinal measurements. RNFL thickness and significance maps showed a constant sensitivity regardless of variations in angular width, area, and depth of the RNFL defects.

Conclusion RNFL thickness and significance maps could be used to distinguish eyes with localized RNFL defects from healthy eyes more effectively than cpRNFL thickness and macular inner retina thickness measurements.

Introduction

Glaucoma is an optic neuropathy characterized by selective and progressive injury to the retinal ganglion cells, leading to loss of the retinal nerve fiber layer (RNFL). The advent of optical coherence tomography (OCT) has allowed quantitative evaluation of RNFL thickness. Circumpapillary RNFL (CpRNFL) measurement using OCT is a widely accepted clinical technique for assessing glaucoma.[1–3] Recently, spectral domain OCT (SD-OCT) with high scan speed and resolution has made regional RNFL imaging and quantitative analysis of a broader area possible.[4–6] Regional RNFL imaging provides topographic thickness information, so a quantitative analysis of the RNFL thickness map is expected to have potential advantages in detecting localized RNFL defects.

Conventional cpRNFL measurements have a similar diagnostic ability to detect localized RNFL defects between time domain OCT and SD-OCT devices.[7,8] In recent studies, the RNFL deviation map from SD-OCT has shown superior performance in detecting RNFL and visual field (VF) defects compared with cpRNFL measurements.[7,9] The RNFL deviation map is composed of red–yellow coded pixels that are modified from the RNFL thickness map compared with a normative database. The RNFL thickness map is a color-scale image containing numeric data of RNFL thickness measurements that may reflect the actual RNFL topographic features more closely. To our knowledge, little is known about the diagnostic performance of RNFL thickness map detecting localized RNFL defects.

The RNFL, which is the axonal fibers of retinal ganglion cells, is distributed all over the retina in a characteristic pattern from the optic nerve to the peripheral retina. Because damage to the RNFL can occur anywhere, $6 \times 6\,mm^2$ regional RNFL imaging may miss RNFL defects outside the scanning regions. Glaucoma leads to thinning of the macular nerve fiber layer (NFL), ganglion cell layer (GCL), and inner plexiform layer (IPL).[10,11] Most of the commercial SD-OCTs can measure these three innermost layers (ganglion cell complex (GCC)) and can detect RNFL defects in GCC substructure imaging.

Therefore, this study was designed to evaluate and compare the ability of SD-OCT in detecting glaucomatous localized RNFL defects in RNFL maps with conventional cpRNFL thickness and macular GCC thickness measurements.

Materials and methods

Participants

For this prospective study, we enrolled patients with localized RNFL defects and normal control subjects who visited the glaucoma center at Hanyang University Medical Center from September 2010 to August 2011. The study protocol was approved by the institutional review board of Hanyang University Medical Center and followed the tenets of the Declaration of Helsinki. Informed consent was obtained from all the participants.

All subjects underwent comprehensive ophthalmic examinations, including a visual acuity test, applanation tonometry, refraction, gonioscopy, fundus examination, pachymetry (SP-3000; Tomey, Nagoya, Japan), standard automated perimetry (Humphrey Field analyzer; Carl Zeiss Meditec, Dublin, CA, USA), and RNFL photography with a confocal scanning laser ophthalmoscope (cSLO, F-10; Nidek, Gamagori, Japan). SD-OCT (3D OCT-2000, software version 7.11; Topcon,

Tokyo, Japan) for RNFL thickness mapping was performed on the same day as cSLO RNFL photography.

The inclusion criterion was the presence of localized RNFL defects on cSLO RNFL photographs associated with glaucoma. Glaucoma was defined as the glaucomatous appearance of the optic nerve head on color fundus photographs (increased cupping, neuroretinal rim notching, optic disc hemorrhage, or cup-to-disc ratio > 0.2 between the eyes) and the presence of VF defects that corresponded to RNFL defects and optic nerve head abnormalities. Preperimetric glaucoma was defined as a localized wedge-shaped RNFL defect clearly visible on cSLO RNFL photography with normal VF results. Control subjects had a normal appearing RNFL, optic nerve heads on cSLO RNFL photographs, VFs tests, and no history of intraocular pressure $> 21\,mm\,Hg$. Eyes with best-corrected visual acuity worse than 20/40, spherical equivalent refractive errors less than -8.0 diopters or greater than $+4.0$ diopters, or the presence of any ophthalmic or neurological disease known to affect RNFL thickness or visual function were excluded. When both eyes of a subject were eligible, one eye was selected at random.

RNFL imaging by cSLO

Wide-angle (60 degree) red-free RNFL photographs were obtained by an F-10 cSLO device using the blue (490 nm) reflectance imaging technique. A conventional red-free RNFL photo camera detects light scattered at the lens or vitreous as well as the signal reflected at the RNFL. Although blue light is affected by media opacities, shorter wavelengths yield higher resolution.[12] The quality and contrast of the images can be improved using a confocal technique.[13]

To quantitatively compare the same region of the RNFL maps, cSLO RNFL photographs were overlaid with 3D OCT-2000 color disc photographs as reference images using Matlab R2010b (The MathWorks Inc., Natick, MA, USA). Image registration was performed by a control point selection tool according to the retinal blood vessels that were matched between the cSLO RNFL photograph and the reference image. The RNFL defect areas were measured within the $5 \times 5\,mm^2$ parapapillary area, and angular measurements were performed on the 3.4-mm diameter circle using ImageJ software (version 1.45; developed by Wayne Rasbands, National Institutes of Health, Bethesda, MD, USA http://rsb.info.nih.gov/ij/). All topographic measurements of RNFL defects were performed by two masked examiners (JWS and KBU) to determine the interobserver intraclass correlation coefficient. The measurements were repeated three times by each examiner to determine the intraobserver coefficient of variation.
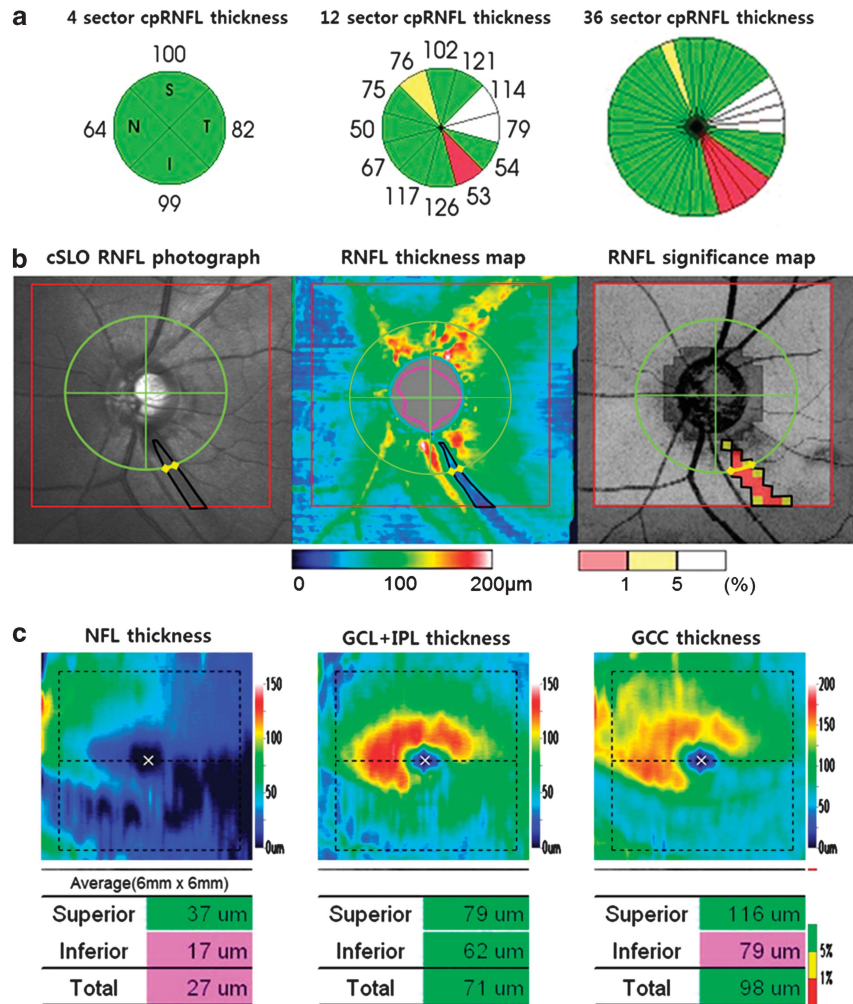
Figure 1 (a) The conventional cpRNFL thickness on the 3.4-mm diameter circle was measured at the 4, 12, and 36 sectors. (b) The RNFL significance map and RNFL thickness map were obtained by Topcon 3D OCT-2000, and the RNFL photograph was captured by a Nidek F-10 cSLO. Each boundary of the RNFL defects was manually delineated. The areas of the RNFL defects were measured on the $5 \times 5\,mm^2$ parapapillary area using ImageJ software (black lines). The angular width and location of the RNFL defects were measured on the 3.4-mm diameter circle (yellow lines). (c) The macular inner retinal thickness is presented as the superior, inferior, and total average components within the $6 \times 6\,mm^2$ macular region.

RNFL imaging by SD-OCT

To obtain the parapapillary RNFL map, a 3D disc scan protocol was applied using a 3D OCT-2000 with an 840 nm wavelength light source, a 5-μm axial image resolution, and a speed of 50 000 A-scans per second. This protocol generated 128 horizontal B-scans each comprised of 512 A-scans on the $6 \times 6\,mm^2$ optic disc region. The built-in analysis software (version 7.11) automatically segmented the RNFL boundary and calculated the RNFL thickness. The optic disc center was automatically detected, and a 3.4-mm diameter circle, which consisted of 1024 A-scans, was placed around the optic disc center. Conventional cpRNFL measurements on the 3.4-mm diameter circle were taken and averages were computed for the 4, 12, and 36 sectors (Figure 1a).

The RNFL defects were defined as ≥ 1 sector at $<5\%$ of the normal level in cpRNFL thickness measurements.

The RNFL thickness map was generated within the $6 \times 6\,mm^2$ parapapillary area with color scales that corresponded with numeric RNFL thickness measurements. Abnormal results based on a comparison of the RNFL thickness to the normative database are displayed in the RNFL significance map. The RNFL significance map is composed of 24×24 pixels within the $5 \times 5\,mm^2$ parapapillary area. Each pixel was coded as yellow if the RNFL measurement was $<5\%$ and $>1\%$ of the normal level or red if it was $<1\%$ of the normal level. All images had image quality factors >50.

To analyze the localized RNFL defects in RNFL thickness and significance maps (yellow and red pixels,

<5% level), the area, angular width, and angular location of the RNFL defects were measured using ImageJ software. A RNFL defect was defined as a wedge-shaped dark blue area surrounding an abrupt color scale change in the RNFL thickness map, and at least five contiguous red or yellow pixels in the RNFL significance map corresponding to photographic localized RNFL defects. The minimum defect size was larger than the diameter of a major retinal vessel. Each boundary was manually delineated, and the RNFL defect areas were measured within the $5 \times 5 \, mm^2$ parapapillary area. The angular width and location of the RNFL defects were measured on a 3.4-mm diameter circle from the optic disc center (Figure 1b). Angles were measured in a clockwise direction in right eyes and in a counterclockwise direction in left eyes, with the temporal equator set at $0°$. The angular measurement was recorded based on right eye orientation, and defects were assigned a clock-hour location according to the measured angles.

A 3D macular vertical scan protocol was used to obtain the macular inner retinal thickness. It consisted of 128 vertical B-scans each comprised of 512 A-scans within the $7 \times 7 \, mm^2$ macular region. The NFL, GCL + IPL, and GCC thicknesses were recorded as the superior, inferior, and total average components within the $6 \times 6 \, mm^2$ macular region (Figure 1c).

Statistical analysis

To evaluate the difference between the normal and glaucomatous eyes with RNFL defects, we compared the means of all the parameters using an independent *t*-test. For the analysis, we grouped borderline and outside normal limits together as abnormal results (abnormality at the fifth percentile). The sensitivity and specificity of each parameter were compared by the Pearson's chi-square test or the Fisher's exact test. To determine the discriminating power for RNFL defects, areas under the receiver operating characteristic curve (AUCs) were calculated. Significant differences between AUCs were assessed using the method described by DeLong *et al*.[14] Reproducibility was assessed by calculating the intraclass correlation coefficients and the coefficients of variation for interobserver and intraobserver topographic measurements, respectively. *P*-values of ≤ 0.05 were considered statistically significant. All statistical analyses were performed using the SPSS software (Version 17.0; SPSS Inc., Chicago, IL, USA).

Results

A total of 136 eyes of 136 participants were included in the study. There were 64 glaucomatous eyes with localized RNFL defects and 72 normal control eyes.

Sixteen eyes had superior RNFL defects, 33 had inferior RNFL defects, and 15 had both superior and inferior RNFL defects (31 superior defects and 48 inferior defects). The average mean deviation of VF tests were significantly different between the normal and localized RFNL defect groups ($-1.47 \pm 0.92 \, dB$ and $-6.26 \pm 4.16 \, dB$, respectively, $P < 0.001$). There were no significant differences in age, gender, laterality, refractive error, and central corneal thickness between the two groups. The interobserver intraclass correlation coefficients in topographic measurements ranged from 0.961 to 1.000 (lower 95% confidence interval 0.909–1.000), and the intraobserver coefficients of variation varied between 0.81 and 5.70%.

Table 1 shows the cpRNFL thickness, macular inner retinal thickness, and angular width and area of RNFL defects in the RNFL maps. Almost all of these quantitative measurements were significantly different between the normal control eyes and the eyes with RNFL defects (all $P < 0.05$, except circumpapillary 9-clock-hour RNFL thickness). The AUCs in terms of quantitative measurements are also presented in Table 1. The angular width and area in the RNFL thickness map (sensitivity 98.4%, specificity 97.0–98.6%, and AUCs 0.985–0.992) and significance map (sensitivity 96.9–98.2%, specificity 95.5–95.8%, and AUCs 0.975–0.983) showed a superior performance in detecting the localized RNFL defects compared with the other parameters (all $P < 0.05$).

The sensitivity, specificity, and AUCs according to the abnormal RNFL criteria (<5% level) provided by the built-in normative database are documented in Table 2. The two parameters with the highest discriminating ability for RNFL defects were the significance map (sensitivity 98.4%, specificity 88.9%, and AUC 0.937) and the thickness map (sensitivity 96.9%, specificity 86.1%, and AUC 0.915). The significance map and the thickness map had a higher sensitivity and AUCs compared with the other parameters (*P*-value 0.001–0.024) except for the 36 sector cpRNFL thickness (sensitivity 92.2%, specificity 87.5%, and AUC 0.898; *P*-value 0.080–0.545). The 4 sector RNFL thickness and GCL + IPL thickness measurements had a high specificity (97.2 and 94.4%, respectively), but sensitivity was low (65.6 and 57.8%, respectively).

The sensitivity for detecting RNFL defects according to the abnormal RNFL criteria (<5% level) was related to the angular width, area, and thickness of the RNFL defects in the cpRNFL measurements (4 sector, 12 sector) and the macular inner retinal measurements (all $P < 0.05$). The RNFL thickness and significance maps showed a relatively constant sensitivity regardless of the variations in angular width, area, and depth of the RNFL defects (all $P > 0.05$ except the relationship between

Table 1 Area under ROC curve between normal controls and eyes with RNFL defects

	Normal eyes (n = 72)	Eyes with localized RNFL defects (n = 64)	P-value	AUCs (95% CI)	Sensitivity/specificity (Sp ≥ 80%)	Sensitivity/specificity (Sp ≥ 90%)
CpRNFL thickness (μm)						
Average	104.2 ± 8.9	84.0 ± 13.9	<0.001	0.890 (0.836–0.944)	75/81	72/90
Quadrant						
Temporal	80.2 ± 11.8	69.8 ± 12.2	<0.001	0.726 (0.641–0.811)	55/81	42/90
Superior	123.9 ± 12.0	101.8 ± 19.4	<0.001	0.840 (0.772–0.908)	78/82	63/90
Nasal	84.6 ± 14.8	74.1 ± 15.8	<0.001	0.694 (0.605–0.783)	48/82	28/92
Inferior	128.1 ± 11.8	90.6 ± 23.4	<0.001	0.910 (0.861–0.959)	83/82	78/90
Clock-hour						
9	69.4 ± 17.4	64.5 ± 12.6	0.06	0.597 (0.500–0.693)	34/81	23/90
10	92.3 ± 13.7	78.1 ± 19.0	<0.001	0.724 (0.637–0.811)	55/81	45/90
11	128.8 ± 19.6	100.1 ± 29.3	<0.001	0.784 (0.705–0.862)	63/81	55/90
12	121.4 ± 19.3	102.7 ± 23.7	<0.001	0.757 (0.676–0.838)	52/81	39/90
1	121.4 ± 15.0	102.9 ± 21.2	<0.001	0.761 (0.682–0.841)	58/83	44/90
2	99.5 ± 17.1	84.2 ± 20.0	<0.001	0.724 (0.638–0.810)	53/81	33/90
3	74.0 ± 16.3	66.4 ± 15.6	0.006	0.646 (0.552–0.739)	36/82	19/92
4	79.9 ± 18.4	71.6 ± 19.4	0.01	0.633 (0.539–0.727)	36/80	20/90
5	111.7 ± 17.9	96.1 ± 21.3	<0.001	0.721 (0.635–0.808)	52/82	38/90
6	133.5 ± 19.2	94.5 ± 27.8	<0.001	0.865 (0.803–0.928)	77/81	72/90
7	138.8 ± 17.4	81.1 ± 35.6	<0.001	0.898 (0.840–0.956)	83/86	81/94
8	78.9 ± 12.4	66.8 ± 15.4	<0.001	0.746 (0.662–0.831)	64/81	41/92
Macular inner retina thickness (μm)						
NFL						
Superior	33.9 ± 5.0	29.3 ± 7.1	<0.001	0.720 (0.631–0.810)	58/81	42/90
Inferior	37.3 ± 4.7	23.5 ± 10.7	<0.001	0.855 (0.782–0.928)	77/82	75/92
Total	35.5 ± 4.4	26.4 ± 7.5	<0.001	0.848 (0.774–0.921)	80/82	75/93
GCL + IPL						
Superior	71.4 ± 6.0	65.5 ± 5.6	<0.001	0.775 (0.697–0.853)	53/81	41/92
Inferior	70.1 ± 5.9	60.0 ± 6.3	<0.001	0.889 (0.833–0.945)	77/83	69/96
Total	70.8 ± 5.1	62.8 ± 5.1	<0.001	0.869 (0.810–0.928)	67/82	61/90
GCC						
Superior	105.4 ± 8.8	94.8 ± 11.6	<0.001	0.771 (0.690–0.851)	59/81	41/90
Inferior	107.3 ± 8.6	83.5 ± 15.9	<0.001	0.888 (0.830–0.946)	80/82	73/90
Total	106.4 ± 8.5	89.2 ± 11.9	<0.001	0.872 (0.811–0.933)	77/82	70/92

	Normal eyes (n = 72)	Eyes with localized RNFL defects (n = 64)	P-value	AUCs (95% CI)	Sensitivity (95% CI)	Specificity (95% CI)
Angular width of RNFL defects (degree)						
Photography	0	32.4 ± 21.1	<0.001	1.0 (0.972–1.000)	100 (94.4–100)	100 (94.9–100)
Thickness map	0.33 ± 1.91	29.4 ± 21.6	<0.001	0.985 (0.946–0.998)	98.4 (91.5–100)	97.0 (89.6–99.6)
Significance map	0.86 ± 4.05	43.9 ± 30.7	<0.001	0.983 (0.938–0.997)	98.2 (90.4–100)	95.5 (87.5–99.1)
Area of RNFL defects (mm²)						
Photography	0	2.46 ± 1.50	<0.001	1.0 (0.973–1.000)	100 (94.4–100)	100 (95.0–100)
Thickness map	0.01 ± 0.04	2.04 ± 1.33	<0.001	0.992 (0.958–1.000)	98.4 (91.6–100)	98.6 (92.5–100)
Significance map	0.05 ± 0.28	2.68 ± 1.76	<0.001	0.975 (0.932–0.994)	96.9 (89.2–99.6)	95.8 (88.1–99.1)

Abbreviations: AUC, area under the receiver operating characteristic curve; CI, confidence interval; GCC, ganglion cell complex; GCL, ganglion cell layer; IPL, inner plexiform layer; NFL, nerve fiber layer; RNFL, retinal nerve fiber layer; ROC, receiver operating characteristic; Sp, specificity.

the angular width of photographic RNFL defects and the significance map). These findings mean that the RNFL thickness and significance maps could detect

smaller and shallower RNFL defects with higher sensitivity than the cpRNFL thickness and macular inner retinal thickness measurements (Table 3).

Table 2 Sensitivity, specificity, and AUCs according to the abnormal RNFL criteria by built-in normative database

| | CpRNFL thickness[a] | | | Topographic RFNL maps | | Macular inner retina thickness | | |
	4 sectors <5%	12 sectors <5%	36 sectors <5%	Thickness map[b]	Significance map <5%	NFL <5%	GCL+IPL <5%	GCC <5%
Sensitivity (95% CI)	65.6 (52.7–77.1)	78.1 (66.0–87.5)	92.2 (82.7–97.4)	96.9 (89.2–99.6)	98.4 (91.6–100)	78.1 (66.0–87.5)	57.8 (44.8–70.1)	76.6 (64.3–86.2)
Specificity (95% CI)	97.2 (90.3–99.7)	94.4 (86.4–98.5)	87.5 (77.6–94.1)	86.1 (75.9–93.1)	88.9 (79.3–95.1)	86.1 (75.9–93.1)	94.4 (86.4–98.5)	90.3 (81.0–96.0)
AUCs (95% CI)	0.814 (0.739–0.876)	0.863 (0.793–0.916)	0.898 (0.835–0.944)	0.915 (0.855–0.956)	0.937 (0.882–0.971)	0.821 (0.746–0.882)	0.761 (0.681–0.830)	0.834 (0.761–0.892)

Abbreviations: AUC, area under the receiver operating characteristic curve; CI, confidence interval; GCC, ganglion cell complex; GCL, ganglion cell layer; IPL, inner plexiform layer; NFL, nerve fiber layer; RNFL, retinal nerve fiber layer.
[a] The RNFL defects were defined as ≥1 sector at <5% of the normal level in cpRNFL thickness measurements.
[b] The RNFL defect was defined as a wedge-shaped dark blue area surrounding an abrupt color scale change in the RNFL thickness map, at least larger than the diameter of a major retinal vessel.

In the group in which localized RNFL defects could not be detected based on the abnormal RNFL criteria of cpRNFL thickness and macular inner retinal thickness parameters, the angular width and area of the RNFL defects on cSLO RNFL photography were significantly smaller, and the average RNFL thickness of the RNFL defects on SD-OCT was significantly greater (all $P < 0.05$). The RNFL thickness and significance maps showed similar results but were not statistically significant because of the small size of the non-detected group (Table 4).

Discussion

RNFL damage can precede detectable optic disc changes and VF loss.[15,16] RNFL abnormalities detected by RNFL photographs were observed in 60% of eyes approximately 6 years before any detectable VF defects.[16] RNFL photography has proven to be the most useful means of detecting RNFL defects.[17] However, RNFL photographs visualize RNFL defects only as areas of reduced optical reflectance compared with thicker areas of the RNFL, and it is difficult to quantify the thickness of the RNFL defect.[18] SD-OCT with high scan speed and resolution provides a three-dimensional RNFL image as a form of topographic RNFL map. In this study, we found that the SD-OCT RNFL thickness map and significance map could discriminate eyes with localized RNFL defects from healthy eyes more effectively when compared with conventional cpRNFL thickness and macular inner retinal thickness measurements.

A previous study reported that the sensitivity and specificity of red-free RNFL photography for discriminating RNFL defects were 80 and 94%, respectively.[17] Conventional cpRNFL measurements have a sensitivity range from 56.5 to 85.9% and a specificity range from 80.0 to 97.4% for detecting localized RNFL defects.[7,8,19,20] In this study, the significance map (sensitivity 98.4%, specificity 88.9%, and AUC 0.937) and the thickness map (sensitivity 96.9%, specificity 86.1%, and AUC 0.915) according to the abnormal RNFL criteria showed a superior performance for detecting the localized RNFL defects. The 36 sector cpRNFL thickness, which was divided by 10-degree intervals, was comparable with the topographic RNFL maps (sensitivity 92.2%, specificity 87.5%, and AUCs 0.898). However, direct comparisons with previous studies may be limited, because the disease severity has a significant effect on the diagnostic performance of OCT, and the study population has different characteristics.[21,22]

RNFL defects are visible on red-free photographs only as shape of reduced optical reflectance when compared with thicker areas of the RNFL.[18] The cpRNFL

Table 3 Sensitivity for detecting RNFL defects according to angular width, area, and thickness of RNFL defects

	No. of eyes	Detection, no. (%)							
		CpRNFL thickness[a]			Topographic RFNL maps		Macular inner retina thickness		
		4 sectors <5%	12 sectors <5%	36 sectors <5%	Thickness map[b]	Significance map <5%	NFL <5%	GCL + IPL <5%	GCC <5%
Angular width of RNFL defects (degrees)[c]									
<10	7	1 (14.3)	1 (14.3)	4 (57.1)	6 (85.7)	6 (85.7)	1 (14.3)	1 (14.3)	1 (14.3)
10 to <20	15	6 (40.0)	8 (53.3)	13 (86.7)	14 (93.3)	15 (100)	10 (66.7)	5 (33.3)	9 (60.0)
20 to <30	11	7 (63.6)	10 (90.9)	11 (100)	11 (100)	11 (100)	9 (81.8)	7 (63.6)	9 (81.8)
≥ 30	31	28 (90.3)	31 (100)	31 (100)	31 (100)	31 (100)	30 (96.8)	24 (77.4)	30 (96.8)
All	64	42 (65.6)	50 (78.1)	59 (92.2)	62 (96.9)	63 (98.4)	50 (78.1)	37 (57.8)	49 (76.6)
P-value		<0.001	<0.001	0.001	0.18	0.04	<0.001	0.003	<0.001
Area of RNFL defects (mm²)[c]									
<1	15	4 (26.7)	5 (33.3)	10 (66.7)	14 (93.3)	14 (93.3)	6 (40.0)	1 (6.7)	6 (40.0)
1 to <2	10	4 (40.0)	6 (60.0)	10 (100)	9 (90.0)	10 (100)	7 (70.0)	5 (50.0)	6 (60.0)
2 to <3	18	15 (83.3)	18 (100)	18 (100)	18 (100)	18 (100)	16 (88.9)	14 (77.8)	16 (88.9)
≥ 3	21	19 (90.5)	21 (100)	21 (100)	21 (100)	21 (100)	21 (100)	17 (81.0)	21 (100)
All	64	42 (65.6)	50 (78.1)	59 (92.2)	62 (96.9)	63 (98.4)	50 (78.1)	37 (57.8)	49 (76.6)
P-value		<0.001	<0.001	0.001	0.34	0.35	<0.001	<0.001	<0.001
Average RNFL thickness (depth) (μm)[d]									
<75	18	16 (88.9)	17 (94.4)	18 (100)	18 (100)	18 (100)	17 (94.4)	16 (88.9)	17 (94.4)
75 to <85	11	10 (90.9)	11 (100)	11 (100)	11 (100)	11 (100)	11 (100)	6 (54.5)	11 (100)
85 to <95	17	13 (76.5)	13 (76.5)	15 (88.2)	17 (100)	17 (100)	13 (76.5)	10 (58.8)	13 (76.5)
≥ 95	18	3 (16.7)	9 (50)	15 (83.3)	16 (88.9)	17 (94.4)	9 (50.0)	5 (27.8)	8 (44.4)
All	64	42 (65.6)	50 (78.1)	59 (92.2)	62 (96.9)	63 (98.4)	50 (78.1)	37 (57.8)	49 (76.6)
P-value		<0.001	0.003	0.19	0.15	0.46	0.003	0.003	0.001

Abbreviations: GCC, ganglion cell complex; GCL, ganglion cell layer; IPL, inner plexiform layer; NFL, nerve fiber layer; RNFL, retinal nerve fiber layer.
[a] The RNFL defects were defined as ≥1 sector at <5% of the normal level in cpRNFL thickness measurements.
[b] The RNFL defect was defined as a wedge-shaped dark blue area surrounding an abrupt color scale change in the RNFL thickness map, at least larger than the diameter of a major retinal vessel.
[c] Angular width and area of RNFL defects were evaluated on red-free RNFL photographs.
[d] Average RNFL thickness of RNFL defects was evaluated on spectral domain optical coherence tomography.

measurements using OCT can be used to evaluate the depth of the RNFL defects. However, it is difficult to visualize the shape of the RNFL defects, because the scanning area is confined to the 3.4-mm circle line. Topographic RNFL imaging by SD-OCT with higher scanning speed and resolution allows simultaneous evaluation of the shape and depth of the RNFL defects. Kim et al[7] reported that the angular width of RNFL defects was related to the detection sensitivity of RNFL defects on SD-OCT. In our study, a similar tendency for the angular width of RNFL defects was observed in the RNFL significance map. However, we found that the sensitivity for detecting RNFL defects in topographic RNFL maps is not affected by the shape (area and angular width) or depth (average RNFL thickness) of the defects, except the angular width in the RNFL significance map. The topographic RNFL maps could detect smaller and shallower RNFL defects with higher sensitivity than cpRNFL thickness and macular inner retinal thickness measurements. The sensitivity for detecting RNFL defects based on cpRNFL thickness and macular inner retinal thickness were closely related to the angular width, area, and depth of the RNFL defects. The RNFL thickness and significance maps have advantages for detecting RNFL defects regardless of the morphological features of the RNFL defects.

CpRNFL scans for assessing glaucoma do not take the full advantages offered by using SD-OCT. SD-OCT offers the ability to take wide regional RNFL measurements with high scan speed and resolution. Therefore, previous studies using the circumpapillary method for evaluating localized RNFL defects or early glaucoma detection reported similar discriminating abilities between time domain OCT and SD-OCT.[7,8,23,24] Analysis of RNFL maps is a proper way to exploit the advantages of SD-OCT. Leung et al[5] reported that a scoring system, which is designed to analyze the RNFL deviation map, significantly improves the diagnostic sensitivity for glaucoma detection at a high level of specificity when compared with cpRNFL measurements. In our study, the significance map and the thickness map showed a superior performance for detecting the localized RNFL

Table 4 Mean angular width and area of photographic RNFL defects and average RNFL thickness according to the presence or absence of RNFL defects

		Not detected		Detected		P-value[a]
		No. of eyes	Mean ± SD	No. of eyes	Mean ± SD	
Angular width of RNFL defects (degree)						
4 sector thickness	(<5% level)	22	16.4 ± 11.7	42	40.8 ± 20.1	<0.001
12 sector thickness	(<5% level)	14	9.9 ± 4.9	50	38.7 ± 19.5	<0.001
36 sector thickness	(<5% level)	5	7.6 ± 4.3	59	34.5 ± 20.6	0.02
Thickness map	[b]	2	8.9 ± 7.1	62	33.2 ± 21.0	0.08
Significance map	(<5% level)	1	3.9	63	32.9 ± 20.9	0.10
NFL thickness	(<5% level)	14	12.2 ± 8.3	50	38.1 ± 20.1	<0.001
GCL + IPL thickness	(<5% level)	27	20.8 ± 15.9	37	40.9 ± 20.5	<0.001
GCC thickness	(<5% level)	15	12.3 ± 8.0	49	38.6 ± 20.0	<0.001
Area of RNFL defects (mm^2)						
4 sector thickness	(<5% level)	22	1.40 ± 1.08	42	3.02 ± 1.40	<0.001
12 sector thickness	(<5% level)	14	0.83 ± 0.49	50	2.92 ± 1.37	<0.001
36 sector thickness	(<5% level)	5	0.72 ± 0.33	59	2.61 ± 1.47	0.005
Thickness map	[b]	2	0.90 ± 0.93	62	2.51 ± 1.50	0.10
Significance map	(<5% level)	1	0.24	62	2.50 ± 1.49	0.10
NFL thickness	(<5% level)	14	1.01 ± 0.70	50	2.87 ± 1.42	<0.001
GCL + IPL thickness	(<5% level)	27	1.53 ± 1.24	37	3.14 ± 1.32	<0.001
GCC thickness	(<5% level)	15	1.04 ± 0.68	49	2.90 ± 1.42	<0.001
Average RNFL thickness (depth) (µm)						
4 sector thickness	(<5% level)	22	94.1 ± 10.7	42	78.7 ± 12.4	<0.001
12 sector thickness	(<5% level)	14	95.4 ± 10.7	50	80.8 ± 13.0	<0.001
36 sector thickness	(<5% level)	5	97.8 ± 9.0	59	82.8 ± 13.6	0.02
Thickness map	[b]	2	102.5 ± 2.1	62	83.4 ± 13.7	0.03
Significance map	(<5% level)	1	104	63	83.7 ± 13.7	0.12
NFL thickness	(<5% level)	14	95.8 ± 10.7	50	80.7 ± 12.9	<0.001
GCL + IPL thickness	(<5% level)	27	90.7 ± 12.3	37	79.1 ± 13.0	0.001
GCC thickness	(<5% level)	15	95.7 ± 10.3	49	80.4 ± 12.8	<0.001

Abbrevaitions: GCC, ganglion cell complex; GCL, ganglion cell layer; IPL, inner plexiform layer; NFL, nerve fiber layer; RNFL, retinal nerve fiber layer; SD, standard deviation.
[a] Mann–Whitney *U* test.
[b] The RNFL defect was defined as a wedge-shaped dark blue area surrounding an abrupt color scale change in the RNFL thickness map, at least larger than the diameter of a major retinal vessel.

defects. The detection of RNFL defects according to the presence or absence criteria on RNFL maps may serve as a useful diagnostic approach for SD-OCT in clinical practice.

The RNFL, which is the axonal fibers of retinal ganglion cells, is distributed all over the retina in a characteristic pattern from the optic nerve to the peripheral retina. Structural damage to ganglion cells and their axons can cause a localized RNFL defect in any distributed area outside the 6 × 6 mm^2 regional RNFL scanning area. Therefore, we evaluated the detecting ability of RNFL defects based on macular inner retinal thickness parameters, which are composed of NFL, GCL, and IPL thickness. The outer retinal layers are hardly affected in glaucoma, whereas the GCL and IPL of the retina, as well as the RNFL, are affected in glaucoma.[11] Recent studies reported that imaging of the macular RNFL is an effective means of detecting macular RNFL defects.[18] The mean thickness of the three innermost

retinal layers is comparable with the cpRNFL thickness in discriminating whether glaucoma is present.[25–27] In this study, the macular inner retinal measurement was comparable with the cpRNFL measurement but showed a poorer ability than the topographic RNFL maps in discriminating RNFL defects.

A limitation of this study is the exclusion of diffuse RNFL defects. In clinical practice, glaucomatous RNFL damages do not always appear in the form of localized defects. Quantitative topographic measurements of diffuse RNFL defects are still a challenging problem in the RNFL thickness map. Manual delineation for the boundary of diffuse RNFL defects is difficult and may include subjective errors. Another limitation of this study is the exclusion of glaucomatous eyes without localized RNFL defects. The present study did not compare a group of glaucomatous eyes without localized RNFL defects with a group of glaucomatous eyes with localized RNFL defects. We can evaluate the abilities of SD-OCT

parameters to distinguish eyes with localized RNFL defects from healthy eyes, but we do not know the ability of those parameters to identify localized RNFL defects.

Segmentation errors are inevitable because of the large amount of sampling scan data for the SD-OCT RNFL maps. Segmentation errors in retinal thickness were previously evaluated by Sadda et al,[28] with severe errors being reported in 13.5% of cases. Clinicians should consider such erroneous cases in evaluating the RNFL thickness. To avoid critical errors, those cases with ambiguous or distorted RNFL defect borders in the SD-OCT RNFL maps were excluded in this study, as well as those with image quality factors <50.

In conclusion, SD-OCT RNFL thickness map and significance map have a superior ability for detecting the localized RNFL defects compared with conventional cpRNFL thickness and retinal inner macular thickness measurements. Combined interpretation of RNFL thickness maps and significance maps provides useful information about glaucomatous RNFL changes in clinical practice. Further studies are needed to evaluate the diagnostic ability of SD-OCT to accurately detect diffuse RNFL defects as well as localized RNFL defects.

Summary

What was known before
- RNFL deviation map was reported as a superior alternative to conventional methods for detecting and monitoring RNFL changes. Little is known about the diagnostic performance of RNFL thickness map.

What this study adds
- RNFL thickness map also have a superior ability for detecting the localized RNFL defects compared with conventional cpRNFL thickness and retinal inner macular thickness measurements.

Conflict of interest

The authors declare no conflict of interest.

Acknowledgements

Author contributions

Study design (KBU, JWS), analysis and interpretation of the data (KBU, JWS), writing the article (JWS), critical revision of the article (KBU, JWS), final approval of the article (KBU), data collection (JWS, WJL, YJK), provision of resources (JWS), statistical expertise (KBU), literature search (KBU, JWS, WJL, YJK), logistic support (KBU).

References

1 Huang ML, Chen HY. Development and comparison of automated classifiers for glaucoma diagnosis using Stratus optical coherence tomography. *Invest Ophthalmol Vis Sci* 2005; **46**: 4121–4129.

2 Parikh RS, Parikh S, Sekhar GC, Kumar RS, Prabakaran S, Babu JG et al. Diagnostic capability of optical coherence tomography (Stratus OCT 3) in early glaucoma. *Ophthalmology* 2007; **114**: 2238–2243.

3 Kim JS, Ishikawa H, Sung KR, Xu J, Wollstein G, Bilonick RA et al. Retinal nerve fibre layer thickness measurement reproducibility improved with spectral domain optical coherence tomography. *Br J Ophthalmol* 2009; **93**: 1057–1063.

4 Ye C, To E, Weinreb RN, Yu M, Liu S, Lam DS et al. Comparison of retinal nerve fiber layer imaging by spectral domain optical coherence tomography and scanning laser ophthalmoscopy. *Ophthalmology* 2011; **118**: 2196–2202.

5 Leung CK, Lam S, Weinreb RN, Liu S, Ye C, Liu L et al. Retinal nerve fiber layer imaging with spectral-domain optical coherence tomography: analysis of the retinal nerve fiber layer map for glaucoma detection. *Ophthalmology* 2010; **117**: 1684–1691.

6 Leung CK, Choi N, Weinreb RN, Liu S, Ye C, Liu L et al. Retinal nerve fiber layer imaging with spectral-domain optical coherence tomography: pattern of RNFL defects in glaucoma. *Ophthalmology* 2010; **117**: 2337–2344.

7 Kim NR, Lee ES, Seong GJ, Choi EH, Hong S, Kim CY. Spectral-domain optical coherence tomography for detection of localized retinal nerve fiber layer defects in patients with open-angle glaucoma. *Arch Ophthalmol* 2010; **128**: 1121–1128.

8 Jeoung JW, Park KH. Comparison of Cirrus OCT and Stratus OCT on the ability to detect localized retinal nerve fiber layer defects in preperimetric glaucoma. *Invest Ophthalmol Vis Sci* 2010; **51**: 938–945.

9 Kang SY, Sung KR, Na JH, Choi EH, Cho JW, Cheon MH et al. Comparison between deviation map algorithm and peripapillary retinal nerve fiber layer measurements using Cirrus HD-OCT in the detection of localized glaucomatous visual field defects. *J Glaucoma* 2012; **21**: 372–378.

10 Tan O, Chopra V, Lu AT, Schuman JS, Ishikawa H, Wollstein G et al. Detection of macular ganglion cell loss in glaucoma by Fourier-domain optical coherence tomography. *Ophthalmology* 2009; **116**: 2305–2314; e1-2.

11 Tan O, Li G, Lu AT, Varma R, Huang D. Advanced Imaging for Glaucoma Study Group. Mapping of macular substructures with optical coherence tomography for glaucoma diagnosis. *Ophthalmology* 2008; **115**: 949–956.

12 Peli E, Hedges 3rd, TR, McInnes T, Hamlin J, Schwartz B. Nerve fiber layer photography. A comparative study. *Acta Ophthalmol (Copenh)* 1987; **65**: 71–80.

13 Woon WH, Fitzke FW, Bird AC, Marshall J. Confocal imaging of the fundus using a scanning laser ophthalmoscope. *Br J Ophthalmol* 1992; **76**: 470–474.

14 DeLong ER, DeLong DM, Clarke-Pearson DL. Comparing the areas under two or more correlated receiver operating characteristic curves: a nonparametric approach. *Biometrics* 1988; **44**: 837–845.

15 Tuulonen A, Lehtola J, Airaksinen PJ. Nerve fiber layer defects with normal visual fields. Do normal optic disc and normal visual field indicate absence of glaucomatous abnormality? *Ophthalmology* 1993; **100**: 587–597

16 Sommer A, Katz J, Quigley HA, Miller NR, Robin AL, Richter RC *et al.* Clinically detectable nerve fiber atrophy precedes the onset of glaucomatous field loss. *Arch Ophthalmol* 1991; **109**: 77–83.

17 Sommer A, Quigley HA, Robin AL, Miller NR, Katz J, Arkell S. Evaluation of nerve fiber layer assessment. *Arch Ophthalmol* 1984; **102**: 1766–1771.

18 Sakamoto A, Hangai M, Nukada M, Nakanishi H, Mori S, Kotera Y *et al.* Three-dimensional imaging of the macular retinal nerve fiber layer in glaucoma with spectral-domain optical coherence tomography. *Invest Ophthalmol Vis Sci* 2010; **51**: 5062–5070.

19 Jeoung JW, Park KH, Kim TW, Khwarg SI, Kim DM. Diagnostic ability of optical coherence tomography with a normative database to detect localized retinal nerve fiber layer defects. *Ophthalmology* 2005; **112**: 2157–2163.

20 Yoo YC, Park KH. Comparison of sensitivities for detecting diffuse and localized retinal nerve fiber layer defects with time-domain optical coherence tomography in patients with glaucoma. *J Glaucoma* 2012, doi: 10.1097/IJG.0b013e31824484b9.

21 Medeiros FA, Zangwill LM, Bowd C, Sample PA, Weinreb RN. Influence of disease severity and optic disc size on the diagnostic performance of imaging instruments in glaucoma. *Invest Ophthalmol Vis Sci* 2006; **47**: 1008–1015.

22 Leite MT, Zangwill LM, Weinreb RN, Rao HL, Alencar LM, Sample PA *et al.* Effect of disease severity on the performance of Cirrus spectral-domain OCT for glaucoma diagnosis. *Invest Ophthalmol Vis Sci* 2010; **51**: 4104–4109.

23 Leung CK, Cheung CY, Weinreb RN, Qiu Q, Liu S, Li H *et al.* Retinal nerve fiber layer imaging with spectral-domain optical coherence tomography: a variability and diagnostic performance study. *Ophthalmology* 2009; **116**: 1257–1263; 63 e1-2.

24 Moreno-Montanes J, Olmo N, Alvarez A, García N, Zarranz-Ventura J. Cirrus high-definition optical coherence tomography compared with Stratus optical coherence tomography in glaucoma diagnosis. *Invest Ophthalmol Vis Sci* 2010; **51**: 335–343.

25 Kim NR, Hong S, Kim JH, Rho SS, Seong GJ, Kim CY. Comparison of macular ganglion cell complex thickness by Fourier-domain OCT in normal tension glaucoma and primary open-angle glaucoma. *J Glaucoma* 2011; **22**(2): 133–139.

26 Seong M, Sung KR, Choi EH, Kang SY, Cho JW, Um TW *et al.* Macular and peripapillary retinal nerve fiber layer measurements by spectral domain optical coherence tomography in normal-tension glaucoma. *Invest Ophthalmol Vis Sci* 2010; **51**: 1446–1452.

27 Kim NR, Lee ES, Seong GJ, Kim JH, An HG, Kim CY. Structure-function relationship and diagnostic value of macular ganglion cell complex measurement using Fourier-domain OCT in glaucoma. *Invest Ophthalmol Vis Sci* 2010; **51**: 4646–4651.

28 Sadda SR, Wu Z, Walsh AC, Richine L, Dougall J, Cortez R *et al.* Errors in retinal thickness measurements obtained by optical coherence tomography. *Ophthalmology* 2006; **113**: 285–293.